Drying-Induced Birefringence of Polyimide Optical Films

Po-Ju Chen and Ta-Jo Liu
Dept. of Chemical Engineering, National Tsing Hua University, Hsinchu, Taiwan, ROC 30043

Ping-Yao Wu, Chi-Fu Tseng, and Chyi-Ming Leu
Material and Chemical Research Laboratories, Industrial Technology and Research Institute, Chutong, Taiwan, ROC 30043

DOI 10.1002/aic.12022
Published online October 28, 2009 in Wiley InterScience (www.interscience.wiley.com).

*Drying-induced birefringence of polyimide film was investigated. The polyimide solutions were coated and dried on two different types of substrates and then removed for optical measurements. The operating window, which was a region for stable and uniform film formation, was determined experimentally. The out-of-plane birefringence (OPBR) was found to increase with decreasing dry film thickness, and the increase became more significant for films less than 10 μm thick. The experimental OPBR results were compared with the predictions of two theoretical models. The results agreed reasonably well with the one-dimensional model of Lei et al. (*J Appl Polym Sci. *2001;81:1000-1013). On the other hand, a simple viscoelastic model, which is an extension of the elastic model of Croll (*J Appl Polym Sci. *1979;23:847-858), could provide clear physical insight, but its applicability was somewhat limited. The effects of several variables such as elasticity number, solidification concentration, yield stress, and mass transfer rate on OPBR were examined.* © 2009 American Institute of Chemical Engineers *AIChE J,* 56: 790–800, 2010
Keywords: birefringence, stress, soluble polyimide, modeling, operating window

Introduction

Polyimide is a polymer that consists of mainly imide groups and aromatic rings. It has several outstanding physical properties such as high thermal stability, good chemical resistance, and strong mechanical properties, because of its highly symmetrical structure and high energy chemical bonds. Various forms of polyimide including fiber, foam, and powder have been widely used in the production of adhesives, coating materials, and more recently, in semiconductor and optic-electronic industries. It is one of the key components in the manufacture of flexible printed circuits and optical films of liquid crystal display (LCD) panels.[1,2]

As polyimide contains a large amount of aromatic rings and has a symmetrical structure, there exists strong molecular interactions, which may create tough resistance for processing. Recently, soluble polyimides have been developed to overcome the processing difficulties.[3] To make soluble polyimide, structural modifications of the polymer chains, such as adding flexible backbones, asymmetric side chains, and bulky monomers have been utilized to reduce the interchains interactions.[4] For optical film applications, a good transmittance is necessary, and this depends on reflection, absorption, and scattering of light of the polymer structure. Hence, the improvement of optical transmittance of polyimide has become the focus of current research.[3–5]

A conventional solvent casting technique is usually adopted to fabricate a soluble polyimide film. In this process, a polyimide film is produced by coating the polymer solution on a moving belt, dried in an oven, and then removed from

Correspondence concerning this article should be addressed to T.-J. Liu at tjliu@che.nthu.edu.tw

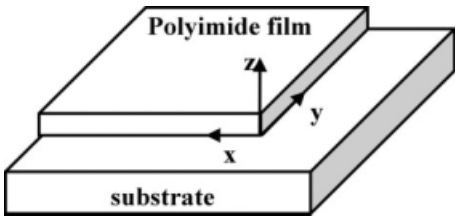

Figure 1. The coordinate system of coating film.

z is the thickness direction.

the belt. During the drying process, the volume of the coated film may shrink due to solvent evaporation. Crystallization, crosslinking, and phase separation may also appear in the process. The volume shrinkage should be isotropic without substrate sticking, but the adhesion between the belt and the polyimide film restricts the horizontal movement of solidified coated film. Accordingly, this volume shrinkage will induce an in-plane stress development.

From a microscopic point of view, the asymmetric shrinkage of coatings implies the appearance of polymer orientation on the film plane. This in-plane orientation induces an out-of-plane birefringence (OPBR). Figure 1 shows the coordinate system of the coating film. Following Greener and Chen[6] the OPBR is defined as,

$$\Delta n_{\mathrm{OP}} \equiv n_z - \frac{1}{2}\left(n_x + n_y\right) \tag{1}$$

and the in-plane birefringence (IPBR) as,

$$\Delta n_{\mathrm{IP}} \equiv n_x - n_y \tag{2}$$

where n_i is the refractive index in the i direction. The polymer has no orientation in the xy-plane because of the symmetric strain developed during drying. Hence, the development of IPBR is nearly zero after drying. On the other hand, the OPBR is proportional to the drying-induced stress[6,7]:

$$\Delta n_{\mathrm{OP}} = C \times \sigma, \tag{3}$$

where σ is the in-plane stress, and C is the stress-optical coefficient of the material. If an optical film has an OPBR, then a phase retardation in the thickness direction, R_{th}, will appear when a light beam passes through the film. This phase retardation is related to the OPBR according to the following equation[8]:

$$R_{\mathrm{th}} = \Delta n_{\mathrm{OP}} \times l \tag{4}$$

where l is the film thickness. In a LCD panel, phase retardation appears when light passes through the liquid crystal. The appearance of phase retardation will reduce the wide-viewing angle and causes the deterioration of the display image. A compensation film made from the soluble polyimide will create the necessary birefringence to offset this phase retardation caused by the liquid crystal, thus, minimizing the phase retardation of the whole LCD panel.[5] Therefore, it is important to control and manipulate the OPBR of polyimide compensation films for different types and arrangements of liquid crystals.

Control of OPBR of polyimide films can be executed by modifying the molecular structure or manipulating the drying process. The drying-stress induced birefringence was discussed by several investigators previously; in 1972, Sosnowski and Weber[9] discovered that the stress developed in the coated film during drying would cause the polymer to lie on the coating plane, resulting in an induction of birefringence. They also found that the birefringence could be reduced by baking the coated films. Prest and Luca[10] observed that the birefringence was dependent upon the orientation of the dominating polarizable group, and found that flexible polymer chains could be helpful in the stress relaxation of the drying film. The effect of birefringence was found to be more significant when the film was thinner. Later, Prest and Luca,[11] Cohen and Reich,[12] and Machell et al.[8] studied the effects of coating thickness, drying temperature, polymer concentration, and molecular weight on the drying-stress induced birefringence. All of their findings were interpreted in terms of a competition between the planar orientation induced by the drying process and the random conformation driven by thermodynamic equilibrium.

To evaluate OPBR, it is necessary to determine the drying-induced stress accurately. Croll[13] developed a simple elastic model to predict the stress. This model is applicable to a purely elastic coating film, but it fails when plastic deformation is not negligible. Lei and coworkers[14,15] proposed a more realistic one-dimensional model to predict the drying-induced stress with both elastic and plastic deformations included. Later Lei et al.[16] extended the model from one- to two-dimensional by including the boundary effects. Greener and Chen[6] showed that the formation of OPBR occurred when the solvent concentration was below a critical value c_{s}^{*}, where the stress started to build up and induce molecular orientation. However, when the solvent concentration dropped below the solidification concentration c_{s}^{**}, polymer chains would no longer move and the formation of OPBR would cease. They also used the two drying-stress models developed by Croll[13] and Lei et al.[14] to calculate the birefringence, and found the predictions based on the latter model were in better agreement with the experimental data of a polystyrene/toluene system.

Soluble polyimide is an expensive material, and controlling the OPBR is a critical operating parameter for optical application. The evaluation of OPBR is solely based on a tedious trial-and-error approach, which would be costly and inefficient. Hence, a good theoretical model for the prediction of OPBR would be highly desirable.

In this study, the drying-stress induced birefringence of soluble polyimide films is experimentally and theoretically investigated. To predict the OPBR after drying, a new simple viscoelastic model, modified from the elastic model of Croll,[13] is developed. In addition, the stress model developed by Lei et al.[14] is also used to compare with the experimental results. The stress model developed by Lei et al.[14] has been found to work for certain polymer systems,[7] but has never been tested for soluble polyimide systems.

Theoretical

The two theoretical models used to compare with the experimental results in this study are described below. The

first one is a modified version of the model proposed by Croll.[13] The second one is the more sophisticated one-dimensional model of Lei et al.[14]

Model A: a modified model of Croll[13]

In this model, it is assumed that in the early stage of the evaporation-controlled drying process, there is no concentration gradient inside the film. Furthermore, the stress starts to build up at $t = t^*$, when the solvent concentration in the film reaches a critical value c_s^*. The variation of film thickness is also assumed to be negligible after the stress build-up. The one-dimensional diffusion equation for the solvent and the corresponding initial and boundary conditions are as follows

$$\frac{\partial c_s}{\partial t} = D\frac{\partial^2 c_s}{\partial z^2} \tag{5}$$

with initial and boundary conditions

$$\text{(i)}\ \ t = t^*, \quad c_s = c_s^* \tag{6a}$$

$$\text{(ii)}\ \ z = 0, \quad \frac{\partial c_s}{\partial z} = 0 \tag{6b}$$

$$\text{(iii)}\ \ z = l, \quad D\frac{\partial c_s}{\partial z} = k_g\left(\mathrm{Hc_s}\big|_{\text{surface}} - c_g^{\infty}\right) \tag{6c}$$

where c_s is solvent molar concentration. The analytical solution of the above system in terms of the average solvent volume fraction $\bar{\phi}_s(t) \equiv \frac{\int_0^l \phi_s(z)dz}{l} = \frac{\int_0^l V_s c_s(z)dz}{l}$ remaining in the drying film is,[17]

$$\frac{\bar{\phi}_s^*(t^*) - \bar{\phi}_s(t)}{\bar{\phi}_s^*(t^*)} = 1 - \sum_{n-1}^{\infty}\frac{2(Sh^*)^2\exp\left(-\psi_n^2 Dt/l^2\right)}{\psi_n^2\left[\psi_n^2(Sh^*)^2 + Sh^*\right]} \tag{7}$$

where V_s is solvent molar volume and ψ_n are the roots of

$$\psi\tan\psi = Sh^* \equiv \frac{k_g Hl}{D^*} \tag{8}$$

which can be found numerically. The power series in Eq. 7 converge rapidly, with only the first few terms necessary to determine $\phi_s(t)$ at time t reasonably accurately.

It is assumed that the drying film exhibits a yield stress after the stress build-up concentration. When the stress exceeds its yield value, the material deforms plastically, following a modified Maxwell model. This mechanical model, which was also used by Lei et al.,[14] consists of a spring connected to two parallel elements: a dashpot and a stick/slip. When the stress is smaller than the yield stress σ_y, the transient stress follows the elastic model of Croll, or

$$\sigma(t) - \sigma(t^*) = \frac{E}{1-\nu}\left\{\varepsilon\left[\bar{\phi}_s(t)\right] - \varepsilon\left[\bar{\phi}_s^*(t^*)\right]\right\} = \frac{E}{1-\nu}\frac{\bar{\phi}_s^*(t^*) - \bar{\phi}_s(t)}{3\left[1-\bar{\phi}_s(t)\right]}, \quad \text{for } \sigma(t) \le \sigma_y \tag{9}$$

and it follows the dashpot movement of the mechanical model when the stress exceeds the yield stress, or

$$\sigma(t) = \sigma(t^*)\exp\left(-\frac{Et}{\mu}\right) = \frac{E}{1-\nu}\varepsilon\left[\bar{\phi}_s^*(t^*)\right]\exp\left(-\frac{Et}{\mu}\right), \quad \text{for } \sigma(t) > \sigma_y \tag{10a}$$

or

$$\sigma(t) = \frac{E}{1-\nu}\varepsilon\left[\bar{\phi}_s(t)\right] = \frac{E}{1-\nu}\left[\frac{\bar{\phi}_s^*(t^*) - \bar{\phi}_s^*(t)}{3\left[1-\bar{\phi}_s(t)\right]} + \varepsilon\left[\bar{\phi}_s^*(t^*)\right]\right]\times\exp\left(-\frac{Et}{\mu}\right), \quad \text{for } \sigma(t) > \sigma_y \tag{10b}$$

The average solvent volume fraction $\phi_s(t)$ in Eqs. 9 and 10b can be estimated from Eq. 7.

Model B: viscoelastic model of Lei et al.[14]

The detailed derivation of the model can be found in the work of Lei et al.[14] In this section, only the governing and the final working equations are presented.

Mass Balance. The dimensionless diffusion equation together with initial and boundary conditions are as follows:

$$\frac{\partial c}{\partial \tau} = \frac{1}{\lambda^2}\frac{\partial}{\partial \eta}\left(\frac{D(c)}{D_0}\frac{\partial c}{\partial \eta}\right) + \frac{\eta}{\lambda}\frac{d\lambda}{d\tau}\frac{\partial c}{\partial \eta} \tag{11}$$

$$c(\eta,0) = 1, \frac{dc(0,\tau)}{d\eta} = 0, \quad \frac{f}{1-\phi_s^0 c}\frac{\partial c}{\partial \eta}(1,\tau) = -Sh\lambda\left(c - c_{eq}\right) \tag{12}$$

$$\frac{d\lambda}{d\tau} = -\phi_s^0 Sh\left(c - c_{eq}\right) \tag{13}$$

$$\lambda(0) = 1 \tag{14}$$

where $c \equiv \frac{c_s}{c_s^0}$ is the dimensionless solvent concentration. This model includes the variation of the film thickness due to solvent evaporation as described by Eq. 13.

Residual Stress. The residual stress σ has to be computed through the film deformation gradients. Lei et al.[14] considered in their analysis the film deformation gradients in both the xy-plane and z-directions, $F_{\parallel}$ and $F_{\perp}$, respectively. Film deformation during drying is caused by volume shrinkage as a result of solvent evaporation, viscoplastic, and elastic deformation. The elastic response is important when the stress is below the yield strength, whereas viscoplastic deformation becomes relevant when the stress exceeds the yield strength. The two overall deformation gradients are assumed to be the product of the three individual deformation gradients, or

$$F_{\parallel} = F_{\parallel}^{s}F_{\parallel}^{e}F_{\parallel}^{vp}, F_{\perp} = F_{\perp}^{s}F_{\perp}^{e}F_{\perp}^{vp} \tag{15}$$

The residual stress σ, built up during the drying process, can be computed from the neo-Hookean equation,

Table 1. Dimensionless Groups and Parameters in Model B

Dimensionless Variables	Dimensionless Groups
Solvent concentration $c \equiv c_s/c_s^0$	Sherwood number $Sh \equiv k_g l_0 H/D_0$
Time $\tau \equiv D_0 t/l_0^2$	Elasticity number $N_{El} \equiv G_0 l_0^2/(\mu_0 D_0)$
Location $\eta \equiv z/l(t)$	Heat-convection number $Hc = \frac{l_0(h^G+h^g)}{D_0\rho^c\hat{C}_p^c}$
Surface position $\lambda \equiv l(t)/l_0$	Evaporation number $Ev = \frac{\Delta H_v}{\hat{C}_p^c(T^G-T_0)}$
Stress $\sigma \equiv (\sigma_\parallel + p_a)/G_0$	Air-temp. number $At = \frac{h^g(T^g-T^G)l_0}{D_0\rho^c\hat{C}_p^c(T^G-T_0)}$
Diffusion function $f \equiv D(c)\ /\ D_0$	Specific-heat number $Sp = \frac{\rho^{sub}\hat{C}_p^{sub}l^{sub}}{\rho^c\hat{C}_p^c l_0}$
Viscosity function $m \equiv \mu(c)/\mu_0$	
Yield stress function $n \equiv k(c)/k_0$	
Modulus function $g \equiv G(c)/G_0$	
Yield stress $\kappa \equiv k_0/G_0$	
Temperature function $\theta \equiv \frac{T-T_0}{T^G-T_0}$	
Equilibrium conc. $c_{eq} \equiv c_g^\infty/(Hc_s^0)$	
Initial volume fraction $\phi_s^0 \equiv V_s c_s^0$	
Stress build-up volume fraction $\phi_s^* \equiv \overline{V}_s c_s^*$	
Solidification volume fraction $\phi_s^{**} \equiv \overline{V}_s c_s^{**}$	

$$\sigma = G\left[\left(F_\parallel^e\right)^2 - \left(F_\parallel^e\right)^{-4}\right] \tag{16}$$

The yielding point Φ can be estimated from the Von Mise criterion:

$$\Phi = \frac{G}{\sqrt{3}}\left|F_\perp\left(F_\parallel^e\right)^2\left[1-\left(F_\parallel^e\right)^{-6}\right]\right| \tag{17}$$

$$\Phi - k = \begin{cases} <0, & \text{no plastic deformation} \\ =0, & \text{critical condition} \\ >0, & \text{continuous yielding} \end{cases} \tag{18}$$

The functions $F_\parallel^{vp} = F_\perp^{vp} = 1$ before yielding, $F_\parallel^{vp}$ can be computed with the following equation after yielding,

$$\frac{1}{F_\parallel^{vp}}\frac{dF_\parallel^{vp}}{d\tau} = \frac{gN_{El}\alpha^3}{6m} \times \left(\frac{1}{\left(\alpha F_\parallel^{vp}\right)^2} - \left(\alpha F_\parallel^{vp}\right)^4 - \sqrt{3}\frac{\kappa n}{g\alpha^3}\frac{1-\left(\alpha F_\parallel^{vp}\right)^6}{\left|1-\left(\alpha F_\parallel^{vp}\right)^6\right|}\right) \tag{19}$$

Hence, parameters σ and Φ can be determined from the deformation gradients $F_\parallel^e$ and $F_\perp$ by Eq. 19 through a series of calculation.[14,15]

Energy Balance. As the cast film is relatively thin, it may be assumed that there is no temperature gradient in the film. Using the model of Alsoy and Duda,[18] the dimensionless energy balance can be written as,

$$\frac{d\theta}{d\tau} = \frac{\mathrm{Hc}[1-\theta] + \mathrm{At} + \mathrm{Ev}\frac{d\lambda}{d\tau}}{\mathrm{Sp}+\lambda} \tag{20}$$

$$\theta(0) = 0 \tag{21}$$

The four dimensionless groups appearing in Eq. 20 are defined in Table 1.

The model equations, combining mass and energy balances with the stress model given above, can be solved numerically by the finite element method.[19] In solving these equations, it is assumed that the physical properties of the soluble polyimide: k_g, h_g, D, H, G, k, $\hat{C}_p$, and ρ are functions of temperature. Accurate predictions of the two models are highly dependent on reliable, meaningful and realistic physical properties, and various parameters in the models as listed in Table 2. Overall, 17 properties and parameters need to be specified for a numerical solution. The formulas used for parameter estimations are given in the section below.

Once the residual stress is obtained from Eq. 16, the OPBR can be calculated by the following stress-optical law[8]:

$$\Delta n_{OP} = C \times \frac{\int_0^l (\sigma dz)}{l}, \quad \text{for } c_s^* < c_s < c_s^{**} \text{ or } \phi_s^* < \phi_s < \phi_s^{**} \tag{22}$$

Parameters Estimation

(1) Stress optical coefficient C (in Eq. 3) is estimated from the formula of Van Krevelen and Hoftyzer[20] developed for the cast film at rubbery state:

$$C = \frac{2\pi\Delta\beta}{45}\frac{(\bar{n}^2+2)^2}{\bar{n}kT}, \quad \Delta\beta = \beta_\parallel - \beta_\perp \tag{23}$$

The difference in polarizability $\Delta\beta$ is determined from the Lorentz-Lorenz equation:

$$\Delta n_{\text{intrinsic}} = \Delta\beta c_m \frac{4\pi}{3}\frac{(\bar{n}^2+2)^2}{6\bar{n}} \tag{24}$$

In this study, the temperature T is replaced by T_{g2} into Eq. 23 as suggested by Greener et al.[7]

(2) Diffusion coefficient D (in Eq. 5) is evaluated from the free volume theory of Vrentas and Duda,[21,22]

$$D(c,T) = D_0(1-\phi_1)^2(1-2\chi\phi) \times \exp\left(-\frac{E_a}{RT}\right)\exp\left(-\frac{\omega_1\hat{V}_1 + \omega_2\xi\hat{V}_2}{\hat{V}_{FH}}\right) \tag{25}$$

$$\hat{V}_{FH} = \omega_1\left(\frac{K_{11}}{\gamma}\right)\left(K_{21} - T_{g1} + T\right) + \omega_2\left(\frac{K_{12}}{\gamma}\right)\left(K_{22} - T_{g2} + T\right) \tag{26}$$

Table 2. Numerical Values of Parameters for Model A and Model B

$V_s = 88.45$ cm^3/mole	$k_g = 1.82 \times 10^{-3}$ cm/s (80°C)
$\frac{K_{12}}{\gamma} = 3.11 \times 10^{-4}$ cm^3/g·K	$H = 0.24$ (80°C)
$K_{22} = 51.6$ K	$\phi_s^{\infty} = 0$
$\hat{V}_2 = 1.33$ cm^3/g (80°C)	$\phi_s^{*} = 0.39$
$T_{g2} = 573$ K	$\phi_s^{**} = 0.34$
$D_0 = 2.48 \times 10^{-4}$ cm^2/s (80°C)	$G = 0.9$ GPa ($c_s = 0$, 80°C)
$\frac{K_{11}}{\gamma} = 3.03 \times 10^{-3}$ cm^3/g·K	$k = 0.0252$ GPa ($c_s = 0$, 80°C)
$K_{21} = -4.7$ K	$\mu = 0.17$ Pa·s (80°C)
$\hat{V}_1 = 0.843$ cm^3/g (80°C)	$\hat{C}_p^{sub} = 1.33$ J/g·K (80°C) for PET
$T_{g1} = 215$ K	$\rho^{sub} = 1.32$ (80°C) for PET
$\xi = 0.23$	$\Delta\hat{H}_v = 402.5$ J/g
$\chi = 0.37$ (80°C)	$C = 0.72$ GPa^{-1}

There are three groups of parameters in Eqs. 25 and 26, which can be determined from the method suggested by Hong[23] as shown below.

(a) Solvent parameters: (D_0, $\frac{K_{11}}{\gamma}$, K_{21}, $\hat{V}_1$, T_{g1})

The specific volume of the solvent is

$$\hat{V}_1 = \frac{V_c(0)}{M_w} \tag{27}$$

Bondi[24] found that

$$V_c(0) \approx 1.3V_w = \frac{1.3 \times V(T)}{\left[1.42 + 0.5\left(T/T_{g1}\right)\right]} \tag{28}$$

where the glass transition temperature of solvent T_{g1} can be found in Ref. 25. The other two parameters $\frac{K_{11}}{\gamma}$ and K_{21} are obtained by fitting the solvent viscosity data as a function of temperature with the Doolittle formula[23]:

$$\ln \mu_1 = \ln A_1 + \frac{\gamma\hat{V}_1/K_{11}}{\left(K_{21} - T_{g1}\right) + T} \tag{29}$$

Finally, D_0 is evaluated from the Dullien equation,[26]

$$\ln\left(\frac{0.124 \times 10^{-16}\tilde{V}_c^{2/3}RT}{\mu_1 M_1 \hat{V}_1}\right) = \ln D_0 - \frac{E(\omega_1 \to 1)}{RT} - \frac{\gamma\hat{V}_1/K_{11}}{\left(K_{21} - T_{g1}\right) + T} \tag{30}$$

(b) Polymer parameters: $\left(\frac{K_{12}}{\gamma}, K_2 2, \hat{V}_2, T_{g2}\right)$

T_{g2} is experimentally determined to be 593 K, and the other two parameters $\frac{K_{12}}{\gamma}$ and K_{22} are estimated with WLF equation.[23,27]

$$\log\left[\frac{\mu_2(T)}{\mu_2\left(T_g\right)}\right] = \frac{\left[-\left(\gamma\hat{V}_2\right)/\left(2.303K_{12}K_{22}\right)\right]\left(T - T_{g1}\right)}{\left(K_{22} - T_{g1}\right) + T} \tag{31}$$

(c) Parameters of interaction: (ξ, χ)

The molar volume ratio ξ is evaluated from the formula proposed by Jiang and Han[28]:

$$\xi = \frac{M_1\hat{V}_1}{0.6224T_{g2}(\mathrm{K}) - 86.95} \tag{32}$$

The polymer-solvent interaction parameter χ is computed using the formula proposed by Bristow and Waston[29]:

$$\chi = 0.35 + \frac{\overline{V}_s}{RT}(\delta_1 - \delta_2)^2 \tag{33}$$

where δ_1 can be found in Ref. 18 and δ_2 is evaluated by the method proposed by Van Krevelen and Hoftyzer.[20]

(3) Mass and heat transfer coefficients k_g (in Eq. 6c) and h^g (Table 1) are estimated by assuming the air flow above the cast film follows the boundary layer theory.[30]

(4) Henry's constant H (in Eq. 6c) follows Henry's law: $H = P_s/c|_{\eta=1}$ in which P_s is evaluated from the Flory-Huggins theory[24]:

$$P_s = P_{vap}\phi_s \exp\left[\phi_s + \chi\left(\phi_p\right)^2\right] \tag{34}$$

The vapor pressure of cyclopentanone P_{vap} is estimated from the Antoine equation[31]:

$$P_{vap}^{0.2}(\mathrm{kPa}) = 0.7407 + 0.01363T\left(^{\circ}\mathrm{C}\right) \tag{35}$$

(5) Limiting concentration c_g^{∞} (in Eq. 6c) is assumed to approach zero in this study.

(6) Onset of stress and solidification concentrations c_s^{*} (in Eq. 6a) and c_s^{**} (in Eq. 22) is evaluated from the data of G as a function of solvent concentration.

(7) Young's modulus E (in Eq. 9) is obtained from $E = 2G(1 + v)$, where $v = 0.5$ for incompressible material.

(8) Viscosity μ (in Eq. 10a) is obtained experimentally.

(9) Molar volume V_s (Table 1) can be found from Ref. 26.

(10) Critical shear stress of yielding k (in Eq. 18) is computed from the formula proposed by Bicerano[32]:

$$k = 0.028 \times E \tag{36}$$

(11) Heat capacities $\hat{C}_p^{sub}$ and $\hat{C}_p^{c}$ (Table 1) are determined as follows:

As suggested by Van Krevelen and Hoftyzer,[20] $\hat{C}_p^{sub}$ is evaluated using the equation for the PET film,

$$\hat{C}_p^{sub} = 0.0046T - 0.2925(\mathrm{J/gK}) \tag{37}$$

In this study, the heat capacity $\hat{C}_p^{sub}$ for the glass substrate is about 0.5. For the coating film, $\hat{C}_p^{c}$ is evaluated from

$$\hat{C}_p^{c} = \phi_s\hat{C}_p^{solv} + \phi_p\hat{C}_p^{poly} \tag{38}$$

(12) Densities ρ^{c} and ρ^{sub} (Table 1) are evaluated from the following equations, as suggested by Van Krevelen and Hoftyzer[20]:

$$\rho^{\text{sub}} = \frac{192.2}{145.09 + 0.094(T - 343)}, \quad T(\text{K}) > 343 \tag{39}$$

$$\rho^{\text{sub}} = \frac{192.2}{143.2 + 0.042(T - 298)}, \quad 298 < T(\text{K}) < 343 \tag{40}$$

For a glass substrate, the specific gravity is nearly constant at 2.6.

The density of the coating film ρ^{c} is evaluated as

$$\rho^{\text{c}} = \phi_{\text{s}}\rho_{\text{s}} + \phi_{\text{p}}\rho_{\text{p}} \tag{41}$$

(13) Heat of vaporization $\Delta\hat{H}_{\text{v}}$ (Table 1) can be found in Ref. 26.

Experimental

Materials

The soluble polyimide was prepared following a patented formulation.[5] Monomers of diamine and dianhydride were added to a solvent under nitrogen atmosphere at the reflux temperature, and polyimide was formed by a polycondensation reaction. The weight-average molecular weight M_{w} and the number-average molecular M_{n} were measured with gel permeation chromatography by dissolving polyimide in *N*-Methyl-2-pyrrolidone (NMP). The value of M_{w} was found to be around 50,000 with a polydispersity index of around 3. The higher molecular weight polymers have been found to hinder stress relaxation during drying, which could cause an increase in OPBR.[11] As the present research was focused on the effects of processing variables on OPBR, the effect of molecular weight was not investigated further. The test solution was prepared by dissolving ~15 wt % of the polyimide in cyclopentanone solvent. Cyclopentanone (Aldrich) has a molecular weight of 84.12 g/mol, specific gravity of 0.95 (25°C), and melting and boiling point of −51.5°C and 131.15°C, respectively. The polyimide solution was hand-coated on two different types of substrates (PET and glass), and then baked in an oven. The dry film was removed from the substrate for optical measurement.

The poly(ethylene) terephthalate (PET) film was manufactured by Toyobo (Code. A4100). It has a specific gravity ρ^{sub} of 1.34, glass transition temperature of 76°C, crystallization temperature of between 130 and 140°C, thermal conductivity of 0.218 W/mK, and heat capacity $\hat{C}_{\text{p}}^{\text{sub}}$ of 1130 J/kg K. The film thickness l^{sub} of 188 μm was cut into A4 sizes for experimental purpose. The glass substrate was provided by Wei-Yen (Taiwan). The thickness l^{sub} is 700 μm, specific gravity ρ^{sub} is 2.6, thermal conductivity is 1.05 W/mK, and heat capacity $\hat{C}_{\text{p}}^{\text{sub}}$ is 880 J/kg K.

Measurements of physical properties

The rheological properties of polyimide solutions were obtained using a TA Rheometrics Fluid Spectrometer RFS2 equipped with a concentric-cylinder sensor at low shear rates. The dry film thickness was determined by a VIS 4-120 optical thickness-measuring instrument (ETA-Optic). Retardation and OPBR were detected by a 21ADH birefringence analysis instrument (Kobra). The glass transition temperature of polyimide T_{g2} was measured by a DSC7 differential scanning calorimetry (Perkin Elmer). The amount of residual solvent was measured by a Q500 thermogravimetry analysis (TGA) device (TA Instruments). Young's modulus and yielding point of optical films were measured by a QC-503B1 Tensile Testing Machine (Cometech).

Experimental procedure

The experimental procedure involved six major stages described below.

(1) *Solution preparation and coating:* The polyimide solution was prepared and hand-coated to an approximate size of 15 × 25 cm^2 on a selected substrate by a laboratory blade coater.

(2) *Drying:* The coated film together with the substrate was dried in a DH-600 oven (YSC) for around 5–10 min, over a temperature range of 40°C to 120°C.

(3) *Peeling:* The dried coating film had to be removed by peeling immediately after solidification under the condition $\phi_{\text{s}} < \phi_{\text{s}}^{**}$. The timing of the removal was critical since the film would be too sticky for peeling if under-dried, and the adhesion between the film and the substrate would be too strong if over-dried.

(4) *Baking:* The peeled film was returned to the oven for further drying, until the residual solvent was less than 3 wt %.

(5) *Thickness measurement:* Once the film was removed from the oven, the quality of the film was visually examined. If there were no defects, then the film thickness was measured. Each data point reported represents an average value of five measurements.

(6) *Measurements of optical properties:* After a piece of dry film of around 15 × 25 cm^2 in size was peeled from the substrate, birefringence was measured at five locations on the sample, with five measurements at each location and the average value taken.

Results and Discussion

The solution viscosity was assumed to depend exponentially on solvent concentration and temperature by the equation:

$$\mu = O(\phi_{\text{s}})Q(T) = c_1 \exp(a_1\phi_{\text{s}}).\exp(b_1/T) \tag{42}$$

The coefficients a_1, b_1, and c_1 were evaluated by least-square fittings, and found to be $a_1 = 36.69$, $b_1 = 4553$, and $c_1 = 3.975 \times 10^{-6}$ (GPa·s), with a confidence level of $R^2 = 0.988$. The fitting is valid for $0.80 < \phi_{\text{s}} < 0.96$ and $20 < T < 80$ (°C).

Figure 2 shows the plot of the shear modulus G against the solvent volume fraction ϕ_{s}. The lowest value of G was measured at a solvent volume fraction $\phi_{\text{s}} = 0.28$. Above this concentration, the sample became too fluid-like, and no meaningful G data could be obtained with the existing tensile testing machine. The shear modulus would drop sharply and approached zero when the solution concentration reached its stress built-up concentration ϕ_{s}^*.[15] For the polyimide solution, the stress built-up concentration was found to be $\phi_{\text{s}}^* = 0.39$. This end-point condition was selected for the

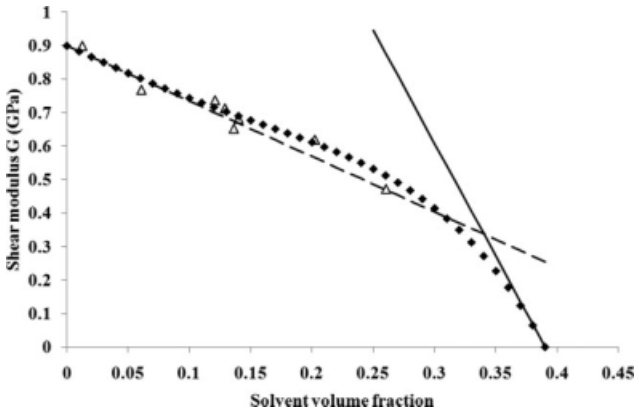

Figure 2. Evaluation of ϕ_s^* and ϕ_s^{**} based on the experimental data of shear modulus G vs. solvent volume fraction ϕ_s.

△: experimental data, ◆: curve fitting, —: tangents of curve-fitting equation at $G = 0$ and $\phi_s = 0$.

polynomial fitting of the experimental data. The best-fitted equation was found to be,

$$G = -55.0\phi_s^4 + 18.0\phi_s^3 - 0.329\phi_s^2 - 1.655\phi_s + 0.901 \quad (43)$$

with $R^2 = 0.976$. It is interesting to observe that the shape of the G vs. ϕ_s curve resembles that of the G vs. T curve for many polymer melts. The glass transition temperature is identified to be the temperature where there is a sudden change of slope of the G curve.[20] Hence, it was assumed in this study that the solidification concentration c_s^{**} could be estimated in the same manner from the intersection of the two tangents drawn respectively from $\phi_s = 0$ and $\phi_s = 0.39$. As shown in Figure 2, the intersection occurs at $\phi_s = 0.35$ or $c_s^{**} = 0.0044$ (mole/cm^3) for the polyimide solution.

The operating windows of soluble polyimide optical film under different drying conditions are shown in Figures 3 and 4 for the PET and glass substrates, respectively. In this context, the operating window is defined as a region of stable and uniform film formation, plotted as film thickness against drying temperature. The temperature range is bounded between the room temperature and the boiling point of the solvent. Initially, the film thickness was set at 25 μm, and

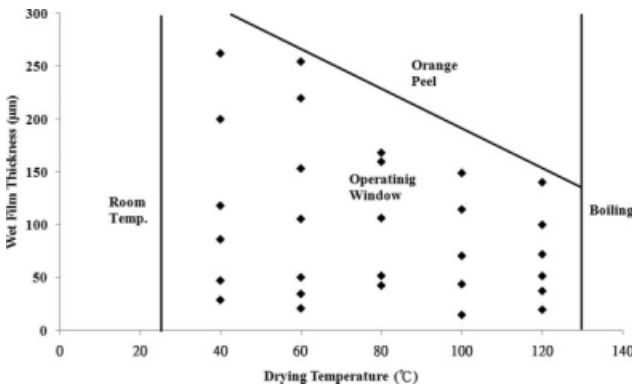

Figure 3. Operating window of drying for PET substrate.

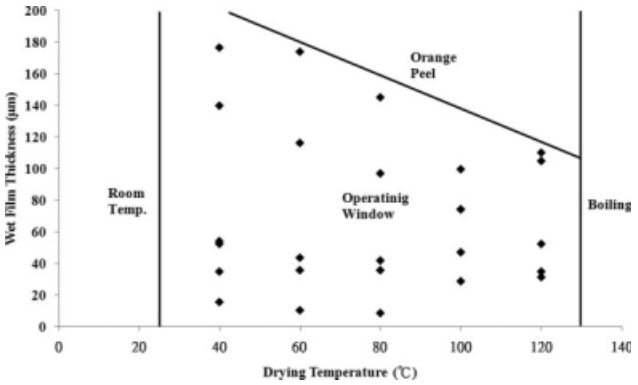

Figure 4. Operating window of drying for glass substrate.

the drying temperature at 40°C. The film thickness was gradually increased at the same temperature until a critical film thickness was reached. Above this thickness, an irregular and corrugated film surface, the so-called orange peel, was observed. A typical "orange peel" surface is shown in Figure 5. This critical wet film thickness is considered as the upper bound of the operating window at 40°C. Other critical wet film thicknesses were similarly obtained by increasing the drying temperature at 20°C intervals. The experiment was terminated when the temperature was close to the boiling point of the solvent.

The results in Figures 3 and 4 indicate that the upper bound film thickness decreases slightly as the drying temperature increases for both PET and glass substrates. However, the appearance of "orange peel" for PET occurs at a slightly thicker film. The rate of heat transfer between the glass substrate and the coated film is slower than the PET substrate, because the former substrate is much thicker than the latter. As a result, the appearance of orange peel would occur at a smaller critical thickness with the glass substrate.

Two mechanisms[33,34] have been proposed to explain the formation of surface corrugation during drying. The first one suggested that a rapid solvent evaporation would produce a dry polymer skin on the free surface and a fluid solution underneath. Continuous evaporation of solvent would cause

Figure 5. Surface appearance of "orange peel."

The wet coated film with the thickness 300 μm was dried at 80°C on glass substrate.

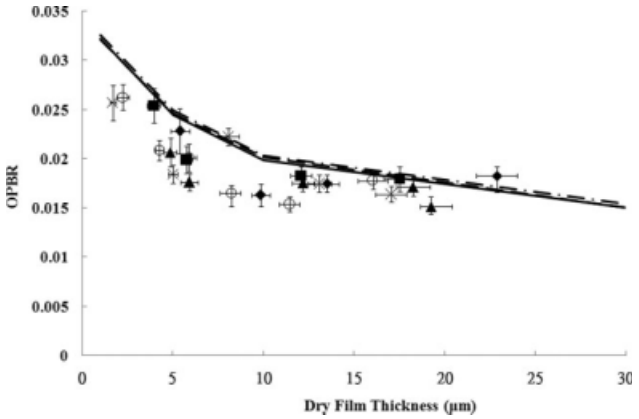

Figure 6. Comparison between the theoretical predictions based on Model B and the experimental results for PET substrate.

◆: 40°C, ■: 60°C, ▲: 80°C, ×: 100°C, ○: 120°C, -.-: theory 40°C, —: theory 80°C, - -: theory 120°C.

the polymer skin to buckle and form a corrugated surface.[33] The second mechanism suggested that the corrugation patterns were the result of an evolution of Raleigh-Bernard or Bénard-Marangoni convective instabilities.[34] It is thought that the "orange peel" observed in this study is due to the first mechanism because it is unlikely for the Marangoni effect to appear under the condition of slow heat transfer through a thick glass substrate.

Comparisons between the theoretical predictions of Model B and the experimental results of OPBR as a function of dry film thickness, over several drying temperatures, are displayed in Figures 6 and 7 for the PET and glass substrates, respectively. Both the theoretical predictions and experimental results indicate that OPBR increases with decreasing drying thickness. Within the experimental uncertainty, there is little variation of OPBR with the drying temperature, as similarly predicted from Model B. On the other hand, the observed OPBR increases more rapidly below a film thickness of 10 μm for both substrates. The theoretical predictions

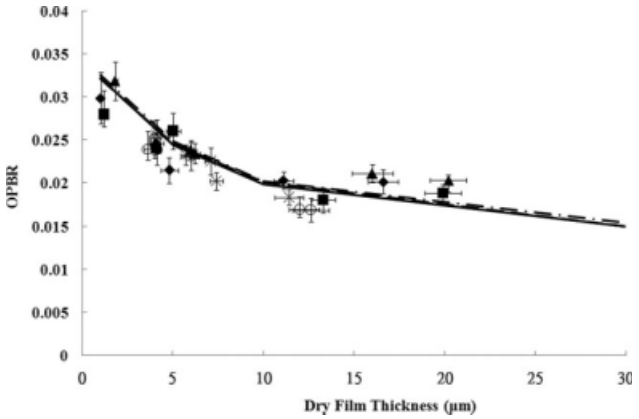

Figure 7. Comparison between the theoretical predictions based on Model B and the experimental results for glass substrate.

◇: 40°C, ■: 60°C, ▲: 80°C, ×: 100°C, ○: 120°C, -.-: theory 40°C, —: theory 80°C, - -: theory 120°C.

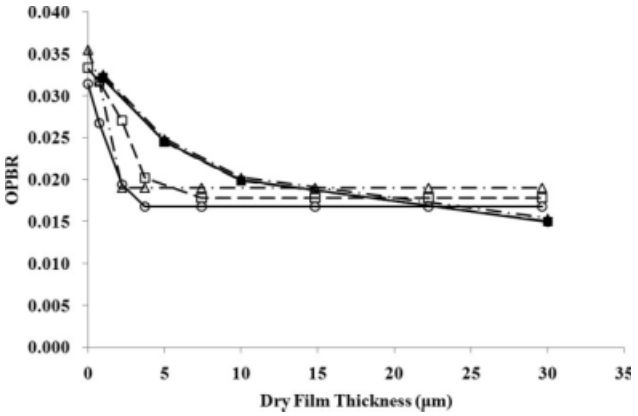

Figure 8. Comparison of the predictions between Model A and Model B.

○: Model A-120°C, □: Model A-80°C, Δ: Model A-40°C, •: Model B-120°C, ■: Model B-80°C, ▲: Model B-40°C.

appear to be closer to the experimental findings for the glass substrate than the PET substrate. Machell et al.[8] reported the experimental findings on the effect of surface energy, and showed that the lower the surface energy for a substrate, the smaller the OPBR. The effect of lowering the surface energy of the substrate is similar to an early removal of the film from the substrate. The present results show that the PET substrate, which has a lower surface energy, produces a smaller OPBR for the same film thickness as compared to the glass substrate. This finding is consistent with the results of Machell et al.[8] Model B assumes that materials move only in the *z*-direction and not on the *xy*-plane, which is expected for a substrate with a high surface energy. Therefore, Model B is more accurate in predicting the OPBR for the glass substrate, which has a higher surface energy than the PET substrate.

As confirmed in Figures 6 and 7 above, Model B is considered to be more accurate for the prediction of OPBR as a function of film thickness. This model is used as a basis to check the validity of Model A. Figure 8 compares the predictions of the two models without the experimental results. Model A predicts that OPBR is independent of the film thickness until the film thickness drops below a critical thickness (around 3–4 μm), below which the OPBR increases rapidly. This prediction is similar to the prediction of Model B in which OPBR continues to decrease slowly throughout the experimental range of film thickness. However, Model A predicts a slight increase in OPBR with decreasing drying temperature, whereas the temperature effect is not evident in the Model B prediction.

Although the prediction of Model A is not as accurate as Model B, it may still provide a meaningful physical interpretation of the drying mechanism. The model predicts that the residual stress σ or OPBR is dependent on four physical parameters: k_g, D, E, and μ. As seen in Eq. 7, when the wet film thickness is increased, the drying time required for $\overline{\phi}_s = \phi_s^*$ to reach $\overline{\phi}_s = \phi_s^{**}$ also increases owing to the higher value of Sh^*. Equation 10 predicts that a longer drying time causes more stress relaxation and reduces the OPBR until the stress reaches the yield strength, beyond which it remains unchanged. On the other hand, a higher

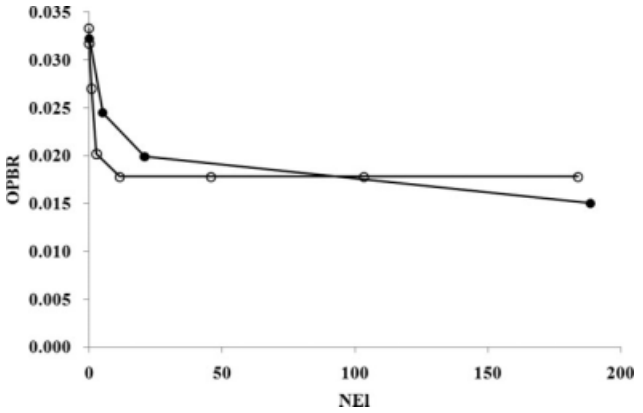

Figure 9. The effect of the elasticity number N_{EL} on OPBR.

○: Model A, •: Model B, other dimensionless parameters: $\kappa = 0.028$, $\phi_s^{**} = 0.34$, $Sh = 1.5$, $A = 14$.

heating temperature results in higher values of k_gH and D, and shortens the drying time. However, a higher heating temperature also decreases the value of E/μ. Hence, the thermal effect on the OPBR is influenced by two competitive factors, i.e., rheological parameter E/μ and drying time. It turns out that for the polyimide system under investigation, the two effects are of similar order of magnitude, thus obscuring any major thermal effect in the system. For other polymer systems, Machell et al.[8] and Prest and Luca[11] found that the thermal effect can be significant.

The effects of elasticity, yield stress, solidification concentration, and external mass transfer on the OPBR were separately examined for the two theoretical models. In the model calculations, several parameters must be specified. The temperature was arbitrarily chosen at $T = 80°C$, and the parameters evaluated at this temperature were $\kappa = 0.028$, $\phi_g = 0.34$, $Sh = 1.5$, and $A = 14$.

The effect of the elasticity number N_{El} on OPBR is shown in Figure 9. The elastic number N_{El} represents the ratio of characteristic drying time to the characteristic time required for stress relaxation. Both models predict a rapid increase in

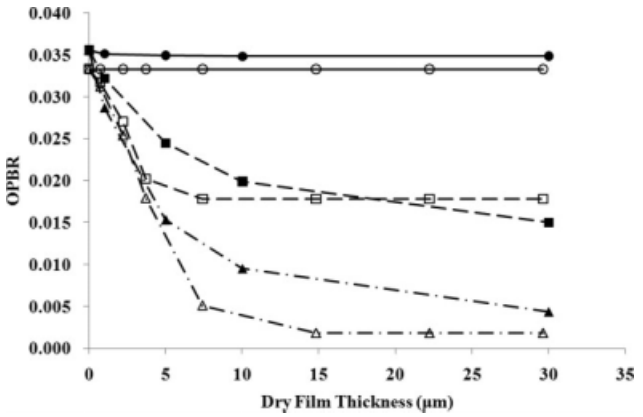

Figure 10. The effect of dimensionless yield stress κ on OPBR.

○: Model A-0.28, □: Model A-0.028, △: Model A-0.0028, ●: Model B-0.028, ■: Model B-0.28, ▲: Model B-0.028. Other dimensionless parameters: $\phi_s^{**} = 0.34$, $Sh = 1.5$, $A = 14$.

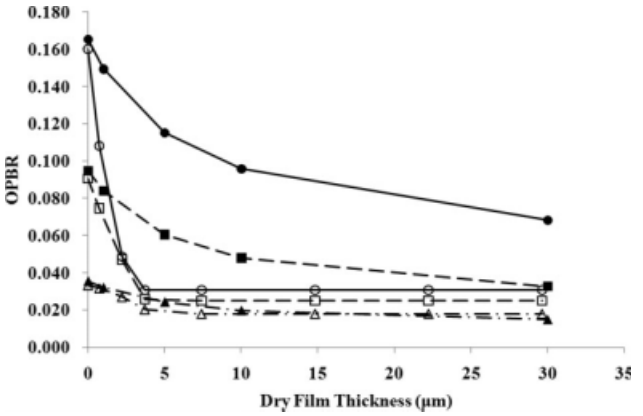

Figure 11. The effect of solidification concentration ϕ_s^{**} on OPBR.

○: Model A-0.34, □: Model A-0.29, Δ: Model A-0.24, •: Model B-0.34, ■: Model B-0.29, ▲: Model B-0.24. Other dimensionless parameters: $\kappa = 0.028$, $Sh = 1.5$, $A = 14$.

OPBR when N_{El} is less than 20. However, Model A predicts that that when $N_{El} > 20$, OPBR is independent of N_{El} and attains a constant value of 1.78×10^{-2}, whereas Model B predicts a gradual decline in OPBR over the same elasticity range.

The effect of the dimensionless yield stress κ on OPBR is presented in Figure 10. The two models predict very similar behavior. The stress cannot easily relax when κ is large, as indicated in the figure for $\kappa = 0.28$, which results in high values of OPBR, independent of the dry film thickness. As κ decreases ($\kappa = 0.028$ and 0.0028), values of OPBR are also reduced. For these two values of κ, Model B also predicts a decline in OPBR with increasing dry film thickness, whereas Model A shows again that OPBR is independent of the dry film thickness beyond certain critical thickness.

The effect of the solidification volume fraction ϕ_s^{**} on OPBR is presented in Figure 11. In general, Model B predicts higher OPBR values than Model A for the same solidification concentration. Both models predict a reduction of OPBR with increasing solidification fraction. For a higher value of ϕ_s^{**}, such as $\phi_s^{**} = 0.34$, OPBR is small, and the variations are less sensitive to the dry film thickness. By contrast, OPBR becomes larger and more sensitive to the dry film thickness for smaller values of ϕ_s^{**}, particularly for the thin film. Physically, ϕ_s^{**} can be considered as the critical volume fraction below which polymer long-chain molecules become motionless. The OPBR can only be developed when the solvent volume fraction is reduced from ϕ_s^{*} to ϕ_s^{**}. Model A assumes that ϕ_s^{*} is very close to ϕ_s^{**} so that the variation of film thickness variation is negligible. However, this assumption is not valid for smaller values of the solidification volume fraction, as the case of $\phi_s^{**} = 0.24$. Hence, it is not expected that Model A will give a realistic prediction of OPBR for high values of ϕ_s^{**}.

The effect of the external mass transfer rate k_g can be demonstrated in Figure 12. At very low drying rates, e.g., $k_g = 1.82 \times 10^{-5}$, Models A and B predict a constant value of OPBR over a wide range of dry film thickness, at 0.018 and 0.012, respectively. At rapid drying, in the case of $k_g = 1.82 \times 10^{-1}$ cm/s, Model B predicts that OPBR increases proportionally as film thickness decreases, whereas Model A

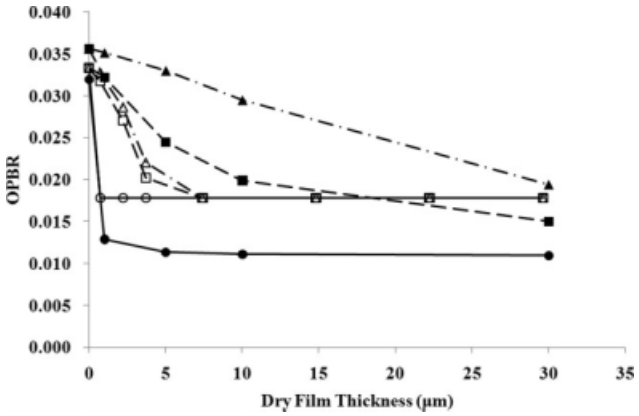

Figure 12. The effect of the external mass transfer coefficient k_g on OPBR.

Δ: Model A-1.82 × 10^{-1}, □: Model A-1.82 × 10^{-3}, ○: Model A-1.82 × 10^{-5}, ▲: Model B-1.82 × 10^{-1}, ■: Model B-1.82 × 10^{-3}, ●: Model B-1.82 × 10^{-5}. Other dimensionless parameters: $\kappa = 0.028$, $\phi_s^{**} = 0.34$.

shows a sharp increase in OPBR only when the dry film thickness is less than 7 μm. Since Model A assumes the drying film behaves as a homogeneous viscoelastic material, it cannot predict accurate OPBR under rapid drying conditions, due to the development of high concentration gradient inside the film. It can be seen from Figure 12 that OPBR can be adjusted effectively by manipulating the external mass transfer rate k_g and the film thickness l. For example, if one desires to make a polyimide film with OPBR $\approx$ 0.02 and a film thickness of 20 μm, it can be achieved by fixing the value of k_g at around 0.003.

The limiting values of OPBR for the soluble polyimide film as predicted by Model B are 0.035 and 0.011 for zero and infinite dry film thickness, respectively. In practice, the maximum wet film thickness is limited by the operating window. Values for the maximum wet film thickness found in Figures 5 and 6 are about 220 μm and 320 μm for the glass and the PET substrates, respectively. The maximum phase retardation for PET and glass substrates as computed from Eq. 4, using a volume fraction of the soluble polyimide of 0.12, are 660.5 nm and 514.8 nm, respectively.

Conclusions

The OPBR of a soluble polyimide film obtained on PET and glass substrates was theoretically and experimentally investigated.

The drying experiment revealed that the OPBR of a soluble polyimide increases slowly as dry film thickness decreases until a critical film thickness of around 10 μm is reached, below which it increases rapidly.

Two theoretical models for the prediction of OPBR were presented and compared with the experimental results. Model A is an extension of the model developed by Croll,[13] Model B is the model developed by Lei et al.[14] Physical parameters of soluble polyimide were evaluated for these two models. Although Model B was found to agree better with the experimental results, Model A is easier to use, and also provides some valuable physical insights on the formation mechanism of OPBR.

The effects of the elasticity number N_{El}, dimensionless yield stress κ, solidification volume fraction ϕ_s^{**}, and external mass transfer rate k_g were also investigated by the two models. Model A provided acceptable predictions except for cases with rapid drying rate and large film thickness variations after stress build-up. Although the limiting values of OPBR as dry film thickness approaches either zero or infinity are predictable from Model B, the actual maximum dry film thickness is limited by the operating window, as presented in Figures 3 and 4. The OPBR of polyimide film can be effectively controlled by adjusting the external mass transfer rate k_g and the film thickness l.

Acknowledgments

This research was supported by the Material and Chemical Laboratory, Industrial Technology and Research Institute, and the National Science Council, ROC, under Grant No. NSC 95-2221-E-007-132-MT3. Comments and suggestions of Prof. Carlos Tiu, Monash University, Australia, are highly appreciated.

Notation

At = air-temperature number
C = stress optical coefficient
$\hat{C}_p$ = heat capacity of coating
c = dimensionless solvent concentration
c_s = solvent molar concentration
c_m = density of molecular units or repeat units
D = diffusion coefficient
D_0 = pre-exponential factor
E = Young's modulus of polyimide coating
E_a = energy required overcoming attractive forces from neighborhood molecules
E_V = evaporation number
F = deformation gradient
f = diffusion coefficient function
G = shear modulus
g = shear modulus function
H = Henry's constant
h = heat transfer coefficient
Hc = heat-convection number
K_{11}, K_{21} = free volume parameters of solvent
K_{21}, K_{22} = free volume parameters of polymer
k = critical shear stress of yielding
k_g = mass transfer coefficient of solvent
l^{sub} = thickness of substrate
l = thickness of coating
m = viscosity function
N_{El} = elasticity number
n = yield strength function
$\bar{n}$ = average refractive index
n_x, n_y = refractive index in x, y directions
O = viscosity function of solvent volume fraction
Q = viscosity function of temperature
R_{th} = phase retardation in thickness direction
Sh = Sherwood number
Sp = specific-heat number
T_g = glass transition temperature
T = temperature of the gas stream
$V_c(0)$ = molar volume of crystalline polymer at 0 K
V_w = Van der Waals volume
V_i = molar volume of component i
$\hat{V}_i$ = specific critical hole free volume of i component
$\hat{V}_{FH}$ = hole free volume of a polymer/solvent mixture

Greek letters

$\beta_{\|}$, $\beta_{\perp}$ = polarizabilities of a polymer segment parallel and perpendicular to the direction of the chain
γ = overlap factor

$\Delta\beta$ = difference in polarizabilities
ΔH_{vs} = heat of vaporization of the solvent
$\Delta n_{intrinsic}$ = intrinsic birefringence of polymer
Δn_{OP} = out-of-plane birefringence of polymer film
Δn_{IP} = in-plane birefringence of polymer film
η = dimensionless z-axis coordinate
θ = dimensionless temperature
κ = dimensionless yield stress
λ = dimensionless coating thickness
μ = viscosity
ν = Poisson ratio
ξ = ratio of the molar volume of the jumping unit of solvent to that of the polymer
ρ = density
σ = stress
τ = dimensionless time
Φ = Von Mise's criterion of yield stress
χ = polymer-solvent interaction parameter
ϕ_i = volume fraction of component i
ω_i = weight fraction of component i

Subscripts

0 = reference state
1 = solvent
2 = polymer
eq = equilibrium
El = elasticity
FH = hole free volume
p = polymer
s = solvent
th = thickness
vap = saturated vapor
$\|$ = parallel
$\perp$ = perpendicular

Superscripts

0 = initial state
c = coating
s = volume shrinkage
sub = substrate
e = elastic deformation
vp = viscoplastic deformation
∞ = far from coating
G = upper gas stream
g = lower gas stream
* = stress starting
** = solidification

Literature Cited

1. Wilson D, Stenzenberger HD, Hergenrother PM. *Polyimides*. New York: Chapman and Hall, 1990.
2. Ghosh MK, Mittal KL. *Polyimides: Fundamentals and Applications*. New York: Marcel Dekker, 1996.
3. Kim YH, Kim HS, Kwon SK. Synthesis and characterization of highly soluble and oxygen permeable new polyimides based on twisted biphenyl dianhydride and spirobifluorene diamine. *Macromolecules*. 2005;38:7950–7956.
4. Liu JG, Nakamura Y, Suzuki Y, Shibasaki Y, Ando S, Ueda M. Highly refractive and transparent polyimides derived from 4,4′-[m-Sulfonylbis(phenylenesulfanyl)] diphthalic anhydride and various sulfur-containing aromatic diamines. *Macromolecules*. 2007;40:7902–7909.
5. Leu CM, Tyan HL, Lee TM. Liquid crystal display device. US Patent 2007/0065603 A1.
6. Geener J, Chen J.*Optical properties of solvent-cast polarizer films for liquid crystal displays.IDMC* Taipei, Taiwan, 2005.
7. Greener J, Lei H, Elman J, Chen J.*Optical properties of solvent-cast polarizer films for liquid crystal display: a viscoelastic modeling framework.SID* Boston, MA, USA:, 2005.
8. Machell J, Greener J, Contestable BA. Optical properties of solvent-cast polymer films. *Macromolecules*. 1990;23:186–194.
9. Sosnowski TP, Weber HP. Thin birefringence polymer films for integrated optics. *Appl Phys Lett*. 1972;21:310–311.
10. Prest WM, Luca DJ. The origin of the optical anisotropic of solvent cast polymeric films. *J Appl Phys*. 1979;50:6067–6071.
11. Prest WM, Luca DJ. The alignment of polymers during the solvent-coating process. *J Appl Phys*. 1980;51:5170–5174.
12. Cohen Y, Reich S. Ordering phenomena in thin polystyrene films. *J Polym Sci*. 1981;19:599–608.
13. Croll SG. The origin of residual internal stress in solvent-cast thermoplastic coatings. *J Appl Polym Sci*. 1979;23:847–858.
14. Lei H, Payne A, McCormick AV, Francis LF, Gerberich WW, Scriven LE. Stress development in drying coating. *J Appl Polym Sci*. 2001;81:1000–1013.
15. Lei H. Flow, deformation, stress and failure in solidifying coatings. PhD Thesis, University of Minnesota, Minnesota, 1999.
16. Lei H, Francis LF, Gerberich WW, Scriven LE. Stress development in drying coatings after solidification. *AIChE J*. 2002;48:437–451.
17. Crank J. *The Mathematics of Diffusion*, 2nd ed. New York: Oxford, 1975.
18. Alsoy S, Duda JL. Drying of solvent coated polymer films. *Drying Technol*. 1998;16:15–44.
19. Zienkiewwicz OC, Taylor RI. *The Finite Element Method*, Vol. 1. London: McGraw-Hill, 1989.
20. Van Krevelen DW, Hoftyzer PJ. *Properties of Polymers*. New York: Oxford, 1976.
21. Vrentas JS, Duda JL. Diffusion in polymer-solvent systems. I. Re-examination of the free-volume theory. *J Polym Sci Part B: Polym Phys*. 1977;15:403–416.
22. Vrentas JS, Duda JL. Diffusion in polymer-solvent systems. II. A predictive theory for the dependence of diffusion coefficients on temperature, concentration, and molecular weight. *J Polym Sci Part B: Polym Phys*. 1977;15:417–439.
23. Hong SU. Prediction of polymer/solvent diffusion behavior using free-volume theory. *Ind Eng Chem Res*. 1995;34:2536–2544.
24. Bondi A. *Physical Properties of Molecular Crystals, Liquids and Glass*. New York: Wiley, 1968.
25. Smallwood IM. *Handbook of Organic Solvent Properties*. New York: Halsted, 1996.
26. Dullien FAL. Predictive equations for self-diffustion in liquids: a different approach. *AIChE J*. 1972;18:62–70.
27. Park KS, Kim D. Determination of diffusion and mass transfer coefficients during drying of solvent-absorbed polymer films. *Polym J*. 2000;32:415–421.
28. Jiang WH, Han R. Prediction of solvent-diffusion coefficient in polymer by a modified free-volume theory. *J Appl Polym*. 1999;77:428–436.
29. Bristow GM, Watson WF. Cohesive energy densities of polymers, Part 1: Cohesive energy densities of rubbers by swelling measurements. *Trans Faraday Soc*. 1958;54:1731–1741.
30. Bird RB, Steward WE, Lightfoot EN. *Transport Phenomena*, 2nd ed. New York: Wiley, 2001.
31. Fisher CH. Equations for correlating vapor pressures with temperature. *J Am Oil Chem Soc*. 2003;80:941–944.
32. Bicerano J. *Prediction of Polymer Properties*. New York: Marcel Dekker, 1993.
33. Pauchard L, Allain C. Buckling instability induced by polymer solution drying. *Europhys Lett*. 2003;62:897–903.
34. Sakurai S, Furukawa C, Okutsu A, Miyoshi A, Nomura S. Control of mesh pattern of surface corrugation via rate of solvent evaporation in solution casting of polymer film in the presence of convection. *Polymer*. 2002;43:3359–3364.

Manuscript received Feb. 24, 2009, and revision received June 24, 2009.